Durability and Mechanical Performance of Elastomeric Membranes Under Thermal–Humidity Aging and Mechanical Stresse

A. Fazli[1*]

[1] RD Department, CTT Group, 3000, avenue Boullé, St-Hyacinthe, QC, Canada J2S 1H9

* *Corresponding author (afazli@gcttg.com)*

Keywords: *Elastomeric membrane; Durability; Degradation mechanisms; Mechanical properties; Creep behavior*

1. Abstract

This study evaluates the long-term durability and mechanical performance of elastomeric composite membranes engineered for demanding building envelope, aerospace, defense, and oil/gas extraction applications. To simulate severe service environments, the membranes were subjected to hygrothermal aging at temperatures ranging from ambient to 85 °C and relative humidity levels up to 90% for exposure cycles of 25 and 50 days. Mechanical characterization including tensile strength, tear resistance, and puncture resistance were conducted before and after accelerated aging to quantify degradation. Post-aging foldability testing was performed to assess flexibility retention, embrittlement resistance, and crack propensity under bending stress. Furthermore, the creep behavior of the membranes was characterized under sustained loading to evaluate long-term deformation resistance as a function of aging duration. Finally, morphological analyses were utilized to correlate microstructural alterations with macro-mechanical degradation mechanisms.

2. Introduction

Elastomers are a class of polymeric materials capable of undergoing large reversible deformations due to the presence of flexible macromolecular chains interconnected through a three-dimensional crosslinked network. Unlike thermoplastics, elastomers exhibit entropy-driven elasticity, where deformation causes polymer chain alignment and recovery occurs through the restoration of thermodynamically favorable random coil conformations [1]. High performance elastomer composites are engineered to withstand extreme temperatures, harsh chemicals, and heavy mechanical stress. The final properties of elastomeric systems are highly dependent on formulation parameters including crosslink density, filler dispersion, curing system, additive migration, and polymer-filler interactions [2]. Owing to their adjustable viscoelastic and damping behavior, elastomers are extensively used in dynamically loaded engineering applications such as seals, gaskets, vibration isolators, conveyor belts, and thermal insulation systems. In these applications, elastomer composites are subjected to complex service conditions involving cyclic mechanical loading, elevated temperatures, oxidative atmospheres, and high humidity exposure, all of which contribute to progressive material degradation and reduced service lifetime [3]. Among commercially available elastomers, ethylene propylene diene monomer (EPDM) rubber has

attracted significant industrial interest due to its excellent thermal stability, weathering resistance, chemical inertness, electrical insulation properties, and resistance to ozone and oxidation [4]. However, EPDM elastomers remain susceptible to thermo-mechanical aging phenomena when exposed to prolonged elevated temperatures and humidity conditions [5]. Exposure to oxygen at high temperatures initiates oxidation reactions that promote polymer chain scission, secondary crosslinking, oxidative group formation, and additive depletion. These molecular-level transformations alter the elastomer network architecture and directly affect macroscopic properties such as tensile strength, hardness, compression set, dimensional stability, and fatigue resistance [6]. Previous investigations have demonstrated that thermal aging can initially increase hardness and modulus due to additional crosslink formation, while prolonged aging eventually causes embrittlement, crack formation, and loss of elasticity [7-9].

The present work was motivated by an industrial problem associated with a vacuum-assisted wood drying system used in the manufacturing of premium hardwood products. As shown in Figure 1, the drying process employs a vacuum kiln equipped with aluminum hot-water heating plates and a flexible elastomeric membrane designed to apply uniform pressure on stacked wood assemblies during drying and cooling operations. During processing, the membrane is exposed to temperatures approaching 150 °C, elevated humidity levels, and vacuum pressures reaching approximately 1,600 lbs/ft² inside the chamber to assist water vaporize which is released at the end of the drying process. Under these conditions, the membrane undergoes repeated thermo-mechanical cycling that progressively deteriorates its structural integrity and functional performance. Therefore, this study focuses on the comparative evaluation of four commercially available elastomer composite membranes with a focus on long-term durability in high-temperature industrial membrane applications. The investigation emphasizes the evolution of mechanical and morphological characterization and dimensional stability as a function of aging exposure.

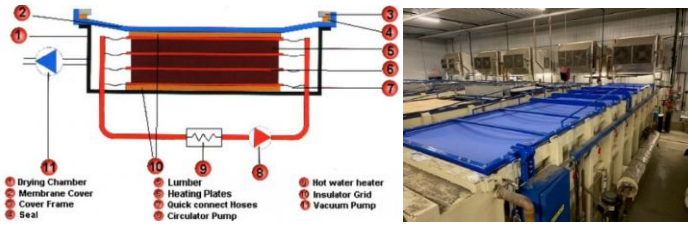

Figure 1. Schematic of vacuum presses and dryer shell.

3. Experimental

3.1. Materials

Four commercially available elastomeric composite membranes were investigated in this study. The materials were selected based on their potential applicability as flexible membranes in vacuum-assisted industrial wood drying systems operating under elevated temperature and humidity conditions. The investigated materials are summarized below (Table 1 and Figure 2).

Table 1 Sample used for testing (all based on EPDM).

Sample	Thickness (mm)	
#1	2.2	filled with 35% CB with lap joints approximately every 60 inches

#2	2.8	filled with 38% CB with glossy surface
#3	3.4	filled with 40% CB offering excellent resistance to ozone, sunlight
#4	3.2	filled with 37% CB combined sulfur/peroxide vulcanization system

#1 **#2** **#3** **#4**

Figure 2. 4 Samples used in this project.

3.2. Accelerated Aging Protocol

Accelerated aging experiments were conducted according to an aging protocol to simulate the operating conditions encountered in industrial vacuum kiln drying systems. Each aging cycle consisted of two sequential conditioning stages:

- **High-temperature/high-humidity stage:** Samples were exposed for 16 h at 85 °C and 90% relative humidity. This stage simulated the operational period during which the elastomeric membrane covers the vacuum wood kiln while the wood releases moisture during drying.

- **Recovery stage:** Samples were subsequently conditioned for 8 h at 23 °C and 50% relative humidity to simulate the cooling and off-duty state of the membrane following completion of the drying process. A total of 50 thermo-hygro aging cycles were performed. Intermediate characterization was conducted after 25 cycles, while final characterization was performed after 50 cycles to evaluate the evolution of material properties as a function of aging exposure duration.

3.3.Characterization

3.3.1. Mechanical Characterization

Mechanical characterization was performed before aging and after 25 and 50 aging cycles in order to quantify the effect of thermo-hygro exposure on the structural integrity and mechanical performance of the elastomeric membranes. Tensile tests (ASTM D412, method A; 500mm/min speed) were performed to determine tensile strength, and elongation at break. Tensile testing also provided the stress values used for determining the applied loading conditions during creep experiments. Low-speed puncture resistance (ASTM F1306; 25mm/min speed) was conducted to evaluate the resistance to localized penetration and mechanical damage under concentrated loading conditions. Tear strength (ASTM D624) was done to evaluate how much force per unit thickness is required to initiate or propagate a tear through a precisely shaped test piece.

3.3.2. Creep and Dimensional Stability Evaluation

A set of specimens was subjected to the same accelerated aging protocol while simultaneously exposed to a constant stress load in order to simulate the tensile stretching experienced by the membranes during vacuum-assisted wood drying operations. The creep loading configuration was designed to maintain a constant tensile stress throughout the thermo-hygro aging exposure. The

applied load for each material was determined from the stress values measured within the initial slope of elastic region (stress vs strain curves) of ASTM D412 results, specifically at 0.5% and 1% strain levels (Table 2). These low-strain values were selected to represent the elastic deformation regime corresponding to realistic membrane stretching during service conditions. The required loading force was calculated using Equation (1):

$$F=\sigma A \tag{1}$$

where F is the applied force (N), σ is the measured stress (Pa), and A is the cross-sectional area of the specimen (m^2). The calculated forces were subsequently converted into equivalent suspended masses according to Equation (2):

$$F=mg \tag{2}$$

where m is the suspended mass (kg) and g is the gravitational acceleration (9.81 m/s^2). The corresponding masses were attached to the lower end of the vertically suspended specimens in order to maintain a constant tensile stress during exposure to elevated temperature and humidity conditions (Figure 3).

Table 2 The calculated weights correspond to the force at 0.5% and 1% deformation.

Sample	Weight at 0.5% deformation (#1)	Weight at 0.5% deformation (#2)
#1	168 g	250 g
#2	115 g	150 g
#3	120 g	180 g
#4	144 g	220 g

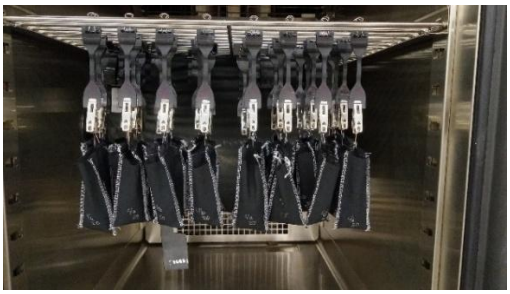

Figure 3 Accelerated aging under load.

3.3.3. Foldability and Cracking Evaluation

An accelerated aging configuration was conducted to evaluate the resistance of the elastomeric membranes to crack formation under localized bending deformation. In this test, the samples were folded and maintained in the folded configuration throughout the aging process to simulate edge and crease deformation occurring under vacuum during kiln operation. The folded specimens were exposed to the same cyclic aging conditions consisting. After aging, visual inspection of the folded regions was conducted to detect cracking, permanent deformation, and surface damage.

3.3.4. Morphological Analysis

Fractured cross-sections of samples after tensile tests were also characterized by SEM at 5 kV. Morphological analysis was then utilized to correlate the observed surface and bulk damage with the degradation of mechanical properties.

4. Results and Discussion

4.1. Mechanical Properties

4.1.1. Tensile Properties

The initial tensile behavior revealed significant differences among the investigated membranes (Table 3). Samples #3 and #4 exhibited the highest tensile strength, with values ranging between 13.7 and 14.76 MPa, indicating a highly reinforced and mechanically stable polymer network. The elongation at break also differed substantially between materials. Sample #4 exhibited the highest elongation values (653–672%), demonstrating superior elastic deformability and network flexibility, while Sample #2 showed the lowest elongation in one testing direction (294%), indicating anisotropic deformation behavior or differences in internal structure orientation. Following thermo-hygro aging, most materials maintained their tensile strength after 25 and 50 cycles. Samples #1 and #4 retained more than 95% of their original tensile performance, while Sample #4 exhibited a progressive increase in tensile stress exceeding 13% after 50 cycles. This behavior is consistent with post-curing and additional crosslink formation during thermal exposure, which increases network rigidity and load transfer efficiency. The most pronounced change was observed for Sample #2, where tensile strength in direction #1 increased from 3.44 MPa to 6.12 MPa after 50 cycles, corresponding to approximately 178% retention relative to the initial condition. This substantial increase suggests that the material initially possessed a relatively low crosslink density and underwent significant structural reorganization or post-vulcanization during aging. The increase in strength was accompanied by an unusual increase in elongation at break after 50 cycles, indicating that the material retained high chain mobility despite network reinforcement. This behavior contrasts with the other membranes, where elongation decreased by approximately 16–43% after aging. The reduction in elongation observed for Samples #1, #3, and #4 is characteristic of thermo-oxidative aging in elastomeric systems. Elevated temperature exposure promotes additional crosslinking reactions and reduces polymer chain mobility, leading to a stiffer network with lower deformability. Sample #3 exhibited the most significant reduction in elongation, decreasing to nearly 55–61% of its original value after aging, indicating substantial hardening of the elastomer matrix. Although this material retained relatively high tensile strength, the marked decrease in extensibility suggests increased brittleness and reduced flexibility after prolonged aging.

Table 3 Results of tensile tests before and after accelerated aging (ASTM D412).

Sample	Property		Initial	After 25 cycles	After 50 cycles
# 1	Strength (MPa)	#a[1]	10.56	10.26	10.23
		#b	**8.97**	9.35	9.69
	Elongation at break (%)	#a	528.4	441.9	409.3
		#b	497.6	442.3	421
# 2	Strength (MPa)	#a	3.44	3.62	6.12
		#b	**3.40**	3.86	3.73
	Elongation at break (%)	#a	458.8	406.3	521.7
		#b	294.4	333.5	304.1
	Strength (MPa)	#a	**13.92**	10.41	11.28

# 3		#b	14.01	11.68	12.06
	Elongation at break (%)	#a	519.7	286.5	296.4
		#b	523	320.4	309.2
# 4	Strength (MPa)	#a	**13.70**	14.88	15.56
		#b	14.76	16.16	15.82
	Elongation at break (%)	#a	671.6	558.6	540.8
		#b	653.8	560.5	523.2

Note 1: Tensile tests were conducted in two orthogonal directions (***a*** and ***b***) to assess the isotropy of the elastomer sheet.

4..1.2. Puncture Resistance

The puncture resistance measurements showed trends consistent with membrane thickness and tensile strength. Sample #3 exhibited the highest initial puncture resistance (256.7 N) and puncture energy (3.51 J), followed by Sample #4. The superior puncture performance of these materials can be attributed to their higher tensile strength, greater thickness, and stronger polymer-filler reinforcement network. Sample #1 exhibited the lowest puncture energy, reflecting its lower thickness and reduced capacity for energy absorption during localized deformation. After accelerated aging, all samples exhibited an increase in puncture resistance, indicating improved resistance to localized penetration following thermo-hygro exposure. The increase ranged from approximately 5.5% for Sample #1 to more than 31% for Samples #2 and #3. These results further support the occurrence of additional crosslinking during aging, which increased resistance against puncture-induced deformation. Samples #1, #3, and #4 exhibited reduced penetration depth after aging, indicating increased stiffness and lower deformability. This trend is characteristic of elastomer hardening caused by thermal aging and increased crosslink density.

Table 4 Results of low-speed puncture resistance tests before and after accelerated aging (ASTM F1306).

Sample	Property	Initial	After 25 cycles	After 50 cycles
# 1	Puncture resistance (N)	137.9	138.33	145.49
	Energy at the point of puncture (J)	1.5	1.3	1.33
	Deformation depth (mm)	26.36	23.34	23.04
# 2	Puncture resistance (N)	141.7	174.1	186.5
	Energy at the point of puncture (J)	2.44	3.26	3.47
	Deformation depth (mm)	42.2	46.55	46.56
# 3	Puncture resistance (N)	256.7	310.67	336.9
	Energy at the point of puncture (J)	3.51	3.52	3.81
	Deformation depth (mm)	37.79	33.01	33.13
# 4	Puncture resistance (N)	199.4	225.1	236.3
	Energy at the point of puncture (J)	3.07	3.27	3.37
	Deformation depth (mm)	38.58	37.23	37.07

4.1.3 Tear Resistance Properties (ASTM D624)

After thermo-hygro aging, samples #1 and #2 exhibited moderate increases in tear strength after 50 cycles, with Sample #2 showed the most significant improvement. This increase suggests that aging promoted additional crosslinking and local hardening near crack initiation regions, thereby improving resistance against tear propagation. Sample #4 remained remarkably stable throughout aging, with variations remaining within approximately ±1% of the initial values. This behavior demonstrates excellent resistance to thermo-hygro degradation and confirms the effectiveness of

the hybrid sulfur/peroxide curing system in maintaining structural integrity under elevated temperature and humidity conditions. The coexistence of sulfur and peroxide crosslinks likely contributed to maintaining both flexibility and thermal stability throughout aging. The reduction in Sample #3 may be associated with aging-induced stiffening and reduced molecular mobility, which can promote localized stress concentration and facilitate crack propagation once tearing is initiated. This behavior is consistent with the significant reduction in elongation observed during tensile testing.

Table 4 Results of Tear Strength tests before and after accelerated aging (ASTM D624)

Sample	Property		Initial	After 25 cycles	After 50 cycles
# 1	Tear Strength (N)	#a[1]	77	84.8	80.9
		#b	73	78	76.1
# 2	Tear Strength (N)	#a	63.6	70.3	74.7
		#b	45.9	45.6	55.6
# 3	Tear Strength (N)	#a	139.5	118.8	134.1
		#b	141.18	128.9	129.9
# 4	Tear Strength (N)	#a	131.2	130.1	129.7
		#b	135.5	135.1	136.9

Note 1: Tear tests were conducted in two orthogonal directions (***a*** and ***b***) to assess the isotropy of the samples.

4.1.4. Creep and Dimensional Stability Under Load

The dimensional changes measured during loaded aging tests provided insight into the creep resistance and long-term dimensional stability of the elastomeric membranes under combined thermo-mechanical loading. In all cases, elongation in the loading direction was accompanied by lateral contraction, consistent with the viscoelastic deformation behavior and Poisson effect characteristic of elastomeric materials subjected to tensile stress. Sample #2 exhibited the best dimensional stability among all investigated materials. Longitudinal deformation remained below 1.1% even after 50 cycles under the highest applied load, indicating excellent creep resistance and stable network structure during thermo-hygro exposure. This behavior suggests that despite its low initial modulus, the material possesses a highly stable viscoelastic response under sustained low-stress loading conditions. Sample #4 exhibited the highest creep deformation, particularly under the higher applied load where elongation reached 6.4% after 50 cycles. Under lower loading conditions, deformation slightly decreased between 25 and 50 cycles, suggesting limited post-curing and hardening effects. However, at higher stress levels, the material exhibited significant viscoelastic deformation, indicating that the applied load exceeded the reinforcing effect generated by additional crosslinking during aging.

Table 5. Dimensional change after accelerated aging.

Sample	Load (g)		After 25 cycles	After 50 cycles
# 1	168g	Length Change (%)	2.4	3.2
		Width Change (%)	0	-2.0
	250g	Length Change (%)	3.6	4.3
		Width Change (%)	0	-4.0
# 2	115g	Length Change (%)	0.7	0.6
		Width Change (%)	0	-2.0
	150g	Length Change (%)	0.6	1.1

		Width Change (%)	0	-4.0
# 3	120g	Length Change (%)	2.2	2.4
		Width Change (%)	0	-2.0
	180g	Length Change (%)	2.8	3.0
		Width Change (%)	-6.0	-4.0
# 4	144g	Length Change (%)	3.8	2.8
		Width Change (%)	-2.0	-2.0
	220g	Length Change (%)	5.0	6.4
		Width Change (%)	-6.0	-2.0

4.1.5. Surface Appearance After Folding Aging

Visual inspection of the folded specimens after 25 and 50 aging cycles revealed no visible cracks or severe surface degradation in any of the four elastomeric membranes (Figure 4). The absence of cracking in the folded regions indicates that the investigated materials retained adequate flexibility and resistance to localized bending stresses despite prolonged exposure to elevated temperature and humidity. This behavior suggests that the thermo-hygro aging conditions used in this study did not induce severe embrittlement or critical surface damage within the elastomer networks. The maintained surface integrity further confirms the suitability of these materials for applications involving repeated flexural deformation and thermo-mechanical cycling under humid industrial environments.

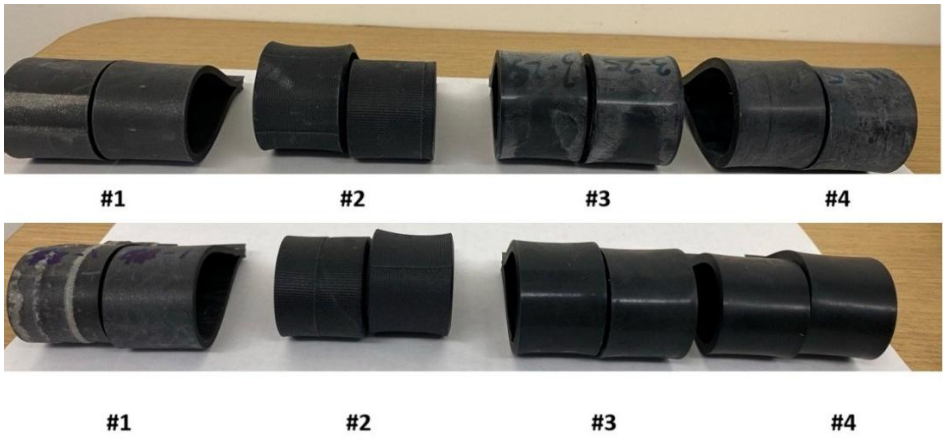

Figure 4. Samples folded after 25 (top) and 50 (bottom) aging cycles.

As shown in Figure 5, SEM was conducted on the tensile-fractured cross-sections of the membranes to correlate microstructural evolution with macroscopic mechanical degradation. In its unaged state, Sample 1 displayed a typical elastomeric fracture with minor filler clusters, transitioning to a rougher topography with microscopic cavities after 50 cycles due to localized thermo-hygro degradation. Sample 2 initially exhibited a uniform and dense cross-section. Post-aging, it developed prominent matrix tearing and localized shear bands, which morphologically substantiates its substantial post-curing effect and enhanced tensile strength. Sample 3 unaged displayed a highly structured fracture surface indicative of strong polymer-filler interactions. However, after 50 cycles, its morphology shifted to a flatter, glassy, and brittle topography, visually validating the severe loss of chain mobility and reduction in elongation at break noted in the mechanical results. In contrast, Sample 4 (Hybrid EPDM) maintained a rugged, tortuous, and highly cohesive fracture path across all aging intervals without evidence of microcracking or

macro-void formation. This structural stability confirms the superior thermal endurance of the combined sulfur/peroxide vulcanization system.

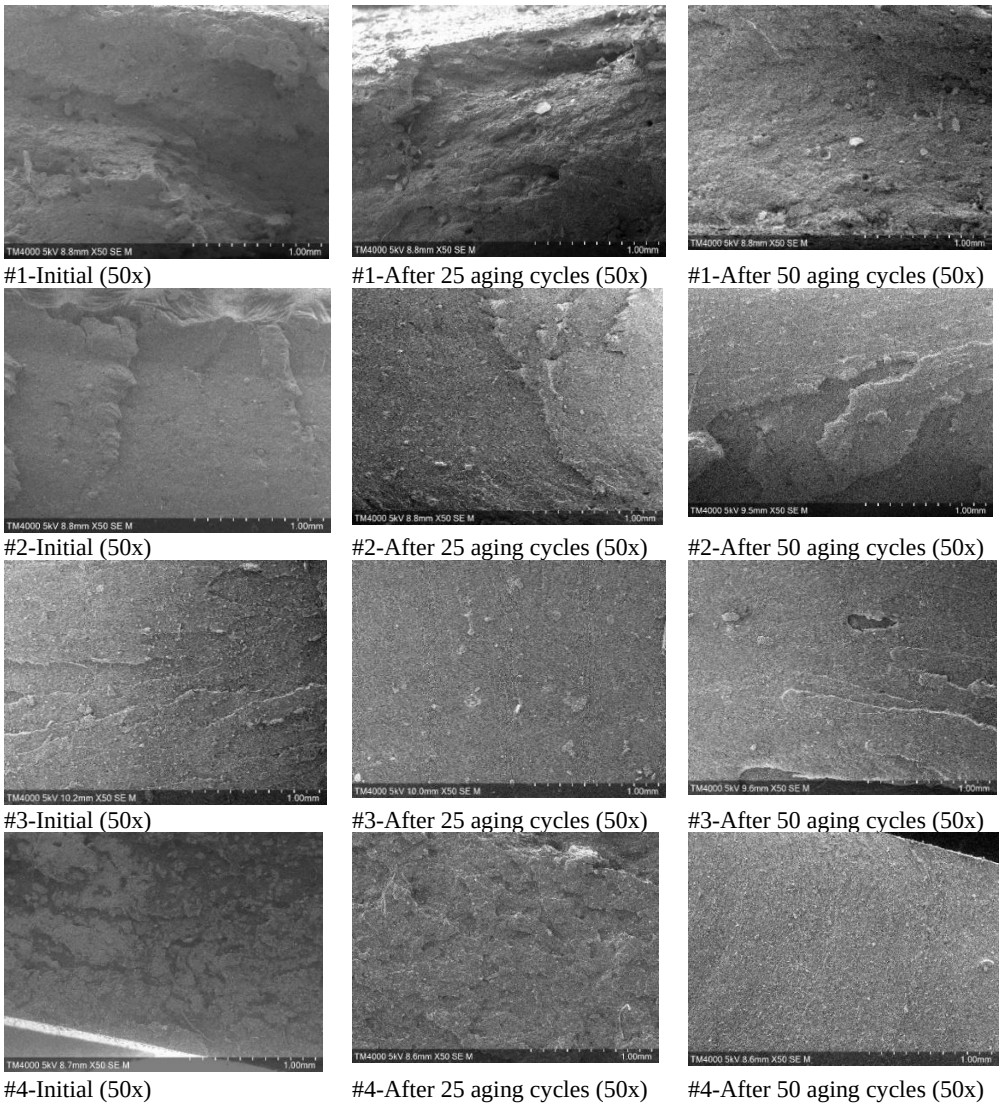

Figure 5. SEM images cross section of ruptured samples tested per ASTM D412 before and after 25, and 50 aging cycles.

5. Conclusion

This study evaluated the effects of cyclic thermo-hygro aging on the mechanical performance and dimensional stability of four EPDM-based elastomeric membranes designed for high-temperature vacuum drying applications. Accelerated aging induced moderate post-curing across all formulations, resulting in increased stiffness alongside enhanced tensile and puncture resistance, while elongation at break decreased due to restricted chain mobility. The extent of these changes was strongly governed by compound formulation, curing system, and specimen thickness. Although all materials successfully resisted localized bending and thermo-hygro fatigue without cracking, distinct performance profiles emerged. The Hybrid EPDM (Sample 4) offered the most balanced combination of strength and durability, whereas Sample 3 exhibited the highest initial mechanical properties but the greatest sensitivity to aging-induced embrittlement. Conversely,

Sample 2 demonstrated superior dimensional stability, minimal creep, and high post-aging ductility, making it advantageous for high-deformation applications, while Sample 1 provided intermediate performance. Overall, these findings demonstrate that while EPDM elastomers can successfully withstand concurrent thermal, humid, and mechanical loads, their long-term behavior remains highly dependent on formulation and crosslinking chemistry. Consequently, Samples 3 and 4 are preferred for optimal overall mechanical performance and aging resistance, whereas Sample 2 is ideal where shape retention and deformation capacity are paramount. Ultimately, this study provides critical formulation-property relationships to guide the selection of elastomer membranes for demanding industrial vacuum drying environments.

6. References

[1] A. Fazli, and D. Rodrigue. "Waste rubber recycling: A review on the evolution and properties of thermoplastic elastomers". *Materials*, Vol. 13, No. 3, pp 782-812, 2020.

[2] M. Maiti, B. Mithun, and A. K. Bhowmick. "Elastomer nanocomposites". *Rubber Chemistry and Technology*, Vol. 81, No. 3, pp 384-469, 2008.

[3] B. Chen, J. Dai, T. Song, and Q. Guan. "Research and development of high-performance high-damping rubber materials for high-damping rubber isolation bearings: A review". *Polymers*, Vol. 14, No. 12, pp 2427-62, 2022.

[4] Y. Lei, J. He, Q. Zhao, and T. Liu. "A nitrile functionalized graphene filled ethylene propylene diene terpolymer rubber composites with improved heat resistance". *Composites Part B: Engineering*, Vol. 134, pp 81-90, 2018.

[5] A. Awwad, D. McDaniel, L. Lagos, J. Rivera, and B. Tansel. "Effect of temperature and aging duration on ethylene propylene diene monomer (EPDM) nonmetallic components used in caustic liquid waste transfer lines". *Engineering Failure Analysis*, Vol. 128, pp 105633-56, 2021.

[6] E. N. M. Chung, M. I. Kittur, A. Andriyana, and P. Ganesan. "On the thermo-oxidative aging of elastomers: A comprehensive review". *Polymer*, Vol. 304, pp 127109-28, 2024.

[7] X. Zhang, J. Li, Z. Chen, C. Pang, S. He, and J. Lin. "Study on thermal-oxidative aging properties of ethylene-propylene-diene monomer composites filled with silica and carbon nanotubes". *Polymers*, Vol. 14, pp 1–11, 2022.

[8] Y. S. Lee, and K. Ha. "Effects of acrylonitrile content on thermal characteristics and thermal aging properties of carbon black-filled NBR composite". *Journal of Elastomers & Plastics*, Vol. 53, No. 5, pp 402-416, 2021.

[9] N. Saintier, G. Cailletaud, and R. Piques. "Cyclic loadings and crystallization of natural rubber: An explanation of fatigue crack propagation reinforcement under a positive loading ratio". *Materials Science and Engineering: A*, Vol. 528, No. 3, pp 1078-1086, 2011.